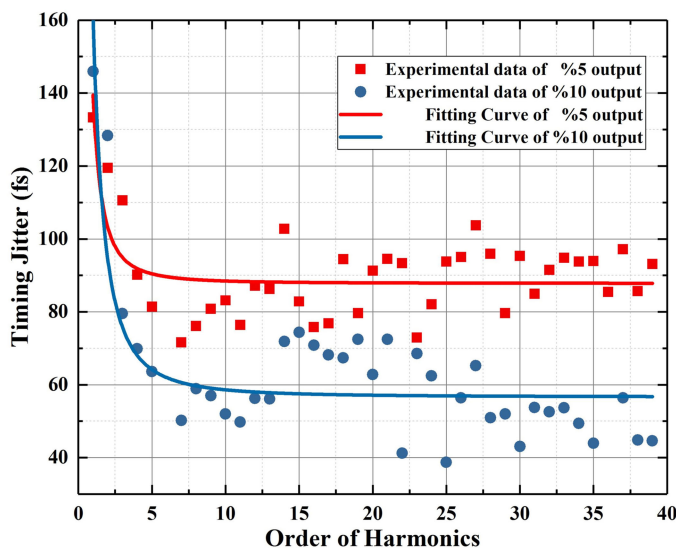


# Experimental Studies on the Noise Properties of the Harmonics From a Passively Mode-Locked Er-Doped Fiber Laser

Volume 11, Number 5, October 2019

Jiazheng Song  
Xiaohong Hu  
Hushan Wang  
Tao Duan  
Yishan Wang  
Yuanshan Liu  
Jianguo Zhang



DOI: 10.1109/JPHOT.2019.2937324

# Experimental Studies on the Noise Properties of the Harmonics From a Passively Mode-Locked Er-Doped Fiber Laser

Jiazheng Song <sup>1,2</sup>, Xiaohong Hu <sup>1</sup>, Hushan Wang <sup>1</sup>, Tao Duan,<sup>1</sup>  
Yishan Wang <sup>1</sup>, Yuanshan Liu <sup>1</sup>, and Jianguo Zhang <sup>1</sup>

<sup>1</sup>State Key Laboratory of Transient Optics and Photonics, Xi'an Institute of Optics and Precision Mechanics, Chinese Academy of Sciences, Xi'an 710119, China

<sup>2</sup>University of Chinese Academy of Sciences, Beijing 100049, China

DOI:10.1109/JPHOT.2019.2937324

1943-0655 © 2019 IEEE. Translations and content mining are permitted for academic research only.

Personal use is also permitted, but republication/redistribution requires IEEE permission.

See [http://www.ieee.org/publications\\_standards/publications/rights/index.html](http://www.ieee.org/publications_standards/publications/rights/index.html) for more information.

Manuscript received February 28, 2019; revised July 16, 2019; accepted August 21, 2019. Date of publication August 28, 2019; date of current version October 28, 2019. This work was supported in part by the National Key R&D Program of China under Grant 2016YFF0200700 and in part by the Natural Science Foundation of China under Grants 61875226 and 61690222. Corresponding author: Jiazheng Song (songjiazheng@opt.ac.cn).

**Abstract:** We experimentally investigate the noise properties of a homemade 586 MHz mode-locked laser (MLL). The variation of the timing jitter versus the harmonic order is measured, which is consistent with the theoretical analyses. The dominant contributions to the timing jitter are detailedly studied by analyzing the phase noises at different harmonic frequencies. For low-order harmonics, the intensity noise and relative-intensity-noise-coupled (RIN-coupled) jitter mainly contribute to the timing jitter, while for high-order harmonics, the amplified spontaneous emission (ASE) noise makes the dominant contribution. Then we find that a higher output ratio has an obvious improvement on reducing the timing jitter and suppressing the phase noise because of the shorter pulse duration and lower net cavity dispersion caused by the higher output ratio. Finally a comparison of the noise performance between the MLL and a commercial signal generator is made, which shows that the optically generated radio-frequency signal (OGRFS) has a lower phase noise at high offset frequencies, however the higher phase noise at low offset frequencies leads to a higher timing jitter than the commercial SG.

**Index Terms:** Passively mode-locked laser, timing jitter, phase noise, harmonic order.

## 1. Introduction

In recent years, passively mode-locked fiber lasers (MLLs) have rapidly developed and been widely used in many application fields, such as optical frequency comb generation [1], [2], high-resolution optical sampling [3], precision optical metrology [4], low noise microwave signal extraction [5], [6], photonics-based radar system [7], and so on. In these systems, the noise property should be improved as much as possible in order to assure the required system performance in terms of sensitivity and precision. Over the past decades, theoretical analysis models related to noise characterization have been built [8]–[13]. D. von de Linde firstly proposed to assess the noise properties of MLLs by measuring the radio-frequency (RF) spectrum of the laser output in his pioneering work in 1986 [8]. A detailed analysis on noise properties under various types of noise

sources was published by Haus and Mecozzi based on soliton perturbation theory [9], which provided fundamental principles for discussing the noise properties of MLLs. Then R. Paschotta studied the quantum-limited noise properties in MLLs via a numerical model, which agrees with the results obtained by using the corrected Haus/Mecozzi analytical model [11], [12]. Based on the well-established theoretical models, the optimization of timing jitter has been experimentally achieved through various approaches [14]–[22]. For example, the reductions of timing jitter through effectively removing Gordon-Haus jitter are demonstrated via managing the intracavity dispersion [14]–[16], or inserting a band-pass filter [17]–[20]. The suppression of intensity noise of a MLL [21] or the optimization of cavity loss [22] also help to lower the timing jitter. Besides, timing jitters are measured at the first four harmonics of an actively MLL by G. Serafino, *et al.* We think the reason the measured timing jitter is independent of the harmonic order is that the intensity noise is much lower than the phase noise of the actively MLL [23]. However, no detailed study on timing jitter and phase noise at different harmonics of a passively MLL has been done so far as we know, which is important in generating low noise high frequency microwave signal from a MLL and some other applications.

In this paper, we experimentally investigate the noise properties of a home-made 586 MHz MLL by using the method proposed in [8], which studies the noise properties by measuring and analyzing the RF power spectra of the optical signals. In Section 2 the basic theoretical model of noise of MLLs is presented, and the experimental setup and the parameters of the MLL used in this paper are also given. In Section 3, we experimentally measure the noise properties of different harmonics, and the detailed discussions are also made. The experimental results show that, for the first five harmonics, the timing jitter progressively decreases with the increase of harmonic order, then the timing jitter fluctuates in a relatively small range ( $\pm 20$  fs) independent of the harmonic order. The fitting curve shows that the variation tendency of the timing jitter is consistent with the theoretical prediction. By analyzing the phase noises of different harmonics, we find that the intensity noise and RIN-coupled jitters mainly contribute to the timing jitter for low-order harmonics, while for high-order harmonics the ASE noise is the dominant noise contribution. The influence of the output ratio of the MLL on timing jitter is studied in Section 4, the results show that a higher output ratio assists in reducing the timing jitter and suppressing the phase noise by narrowing the pulse duration and decreasing the net cavity dispersion. At last, the stabilities of our MLL and a state-of-the-art commercial signal generator (SG) are experimentally compared in Section 5, the advantages and disadvantages of the OGRFSs are presented. The result shows that the OGRFS exhibits a better noise performance at high offset frequencies. However, the higher phase noise at low offset frequencies leads to a higher timing jitter than the commercial SG.

## 2. Theoretical Model and Experimental Setup

The most commonly used approach to analyze the noise properties is proposed by D. von der Linde in [8], which is based on measuring and processing the power spectra of the laser output after impinged on a high-speed photodetector. Firstly, we present the general theory as following. The output pulse from a noiseless pulsed laser can be denoted by  $F_0(t)$  and written as:

$$F_0(t) = \sum_k f(t + kT), \quad (1)$$

where  $f(t)$  denotes the temporal intensity profile of the individual pulse,  $T$  is the period of the pulse train and  $k$  is the harmonic order. For an imperfect MLL, the amplitude and period exhibit random fluctuations. In this case, the laser intensity can be written as:

$$F(t) = F_0(t) + F_0(t)A(t) + \dot{F}_0(t)TJ(t), \quad (2)$$

where  $A(t)$  is a random function which represents the intensity noise and gives the relative deviation from the average pulse amplitude.  $J(t)$  is also a random function which represents the timing jitter and gives the relative deviation from the average pulse repetition time  $T$ . Then, we obtain the power

spectral density (PSD) of the noisy MLL as:

$$S_F(\omega) = \sum_k S_k(\omega) = (2\pi/T)^2 |f(\omega)|^2 \sum_k \left[ \delta(\omega_k) + S_I(\omega_k) + (2\pi k)^2 S_{\Delta T}(\omega_k) \right], \quad (3)$$

where  $\omega_k = (\omega - 2\pi k/T)$  is the angular frequency near around the  $k$ th harmonic frequency,  $\omega$  is the angular frequency,  $f(\omega)$  denotes the Fourier transform of  $f(t)$ ,  $S_I(\omega_k)$  and  $S_{\Delta T}(\omega_k)$  are the PSDs of  $A(t)$  and  $J(t)$ , respectively. From Eq. (3), the noise PSD of the laser is the product of a slowly varying envelope  $|f(\omega)|^2$  and a rapidly varying term that consists of a set of frequency components with constant spacing  $\Delta\omega = 2\pi/T$ . Each frequency component has three different contributions. The first term in the square bracket is a delta function which corresponds to the noiseless power spectrum of an ideal laser. The second term expresses the frequency shifted PSD of the intensity noise. The third term is the timing jitter term that describes the noise originating from the fluctuations of the repetition time  $T$ . The  $k^2$  dependence of this term is an extremely useful property when the noise performance of a laser is characterized. In this paper, we investigate the phase noise and timing jitter at different harmonics from a home-made passively MLL. According to the theoretical models built in [9], [11], [13], the contributions to the timing jitter include the following aspects: (i) the direct influence originating from amplified spontaneous emission (ASE) noise, (ii) the indirect influence caused by ASE noise which is coupled into timing jitter through the intracavity dispersion, namely as Gordon-Haus jitter, (iii) the RIN-coupled jitter through self-steepening effect, (iv) the RIN-coupled jitter determined by Kramers-Krönig relationship (K-K relationship), (v) the RIN-coupled jitter via a slow saturable absorber. The corresponding PSDs are given by Eq. (4).

$$S_{\Delta t, \text{direct}} = 0.53 \frac{\theta h \nu l_{\text{tot}}}{E_p T_{\text{rt}}} \tau_p^2 \frac{1}{(2\pi f)^2}, \quad (4.a)$$

$$S_{\Delta t, \text{indirect}} \approx 0.53 \frac{\theta h \nu l_{\text{tot}}}{E_p T_{\text{rt}}} \Delta v_p^2 \frac{1}{(2\pi f)^2 + \tau_{\text{vc}}^{-2}} \left( \frac{D_2}{f T_{\text{rt}}} \right)^2, \quad (4.b)$$

$$S_{\Delta t, \text{nl}} = \frac{1}{(2\pi f)^2} \left( \frac{\varphi_{\text{nl}}}{\pi T_{\text{rt}} \nu} \right)^2 S_I(f), \quad (4.c)$$

$$S_{\Delta t, g} = \frac{1}{(2\pi \Delta v_g)^2} S_I(f), \quad (4.d)$$

$$S_{\Delta t, s} = \frac{1}{(2\pi f)^2} \left( \frac{s}{T_{\text{rt}}^2} \frac{\partial \Delta T}{\partial s} \right)^2 S_I(f). \quad (4.e)$$

Here,  $\theta$  is the spontaneous emission factor of the gain fiber,  $\nu$  is the frequency of the optical pulse,  $E_p$  is the pulse energy,  $l_{\text{tot}}$  is the total intracavity losses per round trip,  $\tau_p$  is the pulse duration,  $T_{\text{rt}}$  is the round-trip time,  $f$  is the noise offset frequency,  $D_2$  is the net group delay dispersion (GDD) in the cavity and  $\tau_{\text{vc}}$  is the filter time constant related to  $\Delta v_g$  and  $\Delta v_p$ , which are gain bandwidth and pulse bandwidth respectively.  $\varphi_{\text{nl}}$  is the peak nonlinear phase shift,  $s$  is the saturation parameter of the saturable absorber (ratio of intracavity pulse energy and saturation energy of the saturable absorber) and  $\partial \Delta T / \partial s$  is the temporal shift on the saturation parameter.

To measure the noise spectrum of a pulse laser, a high-speed photodetector is used to transfer the optical pulse train into the RF signal which is then analyzed by a signal analyzer. The obtained noise spectrum is composed of the last two terms in Eq. (3). The phase jitter  $\Delta\varphi_k$  of the pulse train can be calculated by Eq. (5).

$$\Delta\varphi_k = \sqrt{\int_{-\infty}^{+\infty} S_k(f) df} = \sqrt{2 \int_{f_{\text{min}}}^{f_{\text{max}}} L_k(f) df}, \quad (5)$$

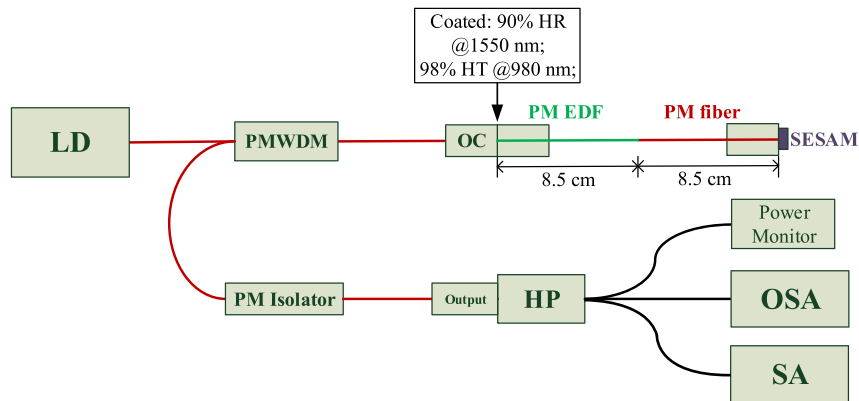


Fig. 1. A schematic diagram of the experimental setup. (Red line: optical signal path, black line: electrical signal path).

$L_k(f)$  denotes the intensity of the phase noise spectrum in dBc/Hz which can be obtained directly by using the spectrum analyzer. Then, the timing jitter can be expressed as:

$$\Delta t_k = \frac{\Delta \varphi_k}{2\pi k f_r}. \quad (6)$$

The parameter  $f_r$  in Eq. (6) represents the pulse repetition rate of the tested laser. Combining Eqs. (3)–(5), for the case of  $k = 0$ , the noise spectrum has no contribution from the temporal jitter, which means that we can directly obtain the power spectrum of the intensity noise by measuring the noise spectrum of the zero frequency component. On the other hand, for sufficient high harmonics, the noise spectra are dominated by ASE noise. Under this circumstance, the influence of the intensity noise is reduced and we find that the timing jitter approaches to a certain value which will be presented in Section 3 of our paper.

A schematic diagram of the experimental setup is depicted in Fig. 1. The laser cavity consists of an 8.5 cm polarization-maintaining (PM) EDF (Liekki Er80-4/125-PM), an 8.5 cm single mode PM fiber (PM980-HP, Nurferrn), a coated PM fiber ferrule and a piece of semiconductor saturable absorbing mirror (SESAM). The PM gain fiber is fusion-spliced to the PM fiber and both ends of the fiber assembly are secured in ceramic ferrules and flat polished. Here we adopt PM980-HP instead of PM1550 single mode PM fiber in the cavity because the  $5.5 \mu\text{m}$  core diameter (CD) of PM980-HP is much more close to the  $4\text{-}\mu\text{m}$  CD of PM EDF. This can greatly reduce the energy loss at the splice joint between the PM single mode fiber and PM EDF. The polished end of the gain fiber is connected to a coated PM fiber ferrule through a mating sleeve. The coated PM fiber ferrule, adopted as an output coupler (OC), has a high reflectivity (HR) of 90% (95% for the laser used in Section 4) at 1550 nm as well as a high transmittance (HT) of over 98% at 976 nm to increase the pump efficiency. The polished end of the PM fiber is butt-coupled to a SESAM which is used to realize mode-locking. The SESAM produced by Batop GmbH has 18% modulation depth, 30% absorbance, 5 ps recovery time and  $1 \text{ mJ/cm}^2$  damage threshold. The pump light provided by a 976 nm laser diode (LD) is injected into the cavity through a PM wavelength division multiplexer (PMWDM) and the coated PM fiber ferrule. The optical pulses are outputted through a PM isolator which is used to eliminate the influence of unabsorbed pump light. The optical spectrum of the output pulses is measured by an optical spectrum analyzer (OSA, model: AQ6370D, YOKOGAWA). The RF spectrum is detected by a high-speed photodetector (HP, model: UPD-15-IR2, ALPHALAS) and monitored by a spectrum analyzer (SA, model: FSW50, Rohde & Schwarz).

Figure 2(a) shows the spectra of the optical pulses from the laser with 10% (green solid line) and 5% (red solid line) OCs. The optical spectra are both measured at a pump power of 327 mW while the output powers are 1.979 and 1.089 mW. The central wavelengths are 1553.4 and 1549.9 nm with 3 dB spectral bandwidths of 10.1 and 8.5 nm, respectively. Since the two lasers adopt the same

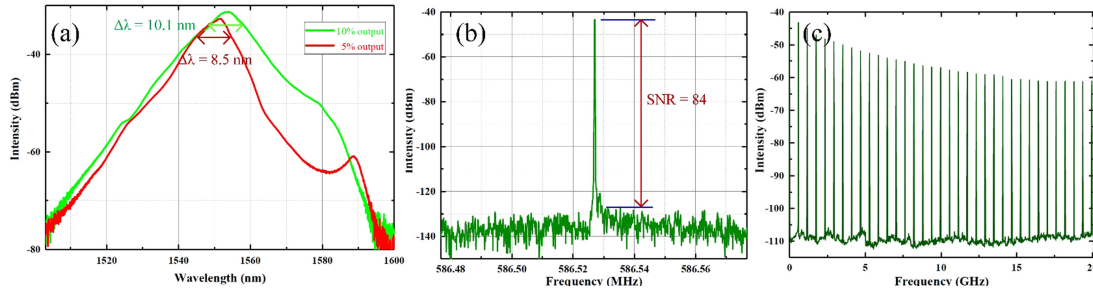


Fig. 2. (a) The optical spectra of the MLLs (green line: 10% output ratio, red line: 5% output ratio), (b) RF spectrum of the MLL, (c) RF spectrum of the MLL with a wide span.

configuration which result in an identical pulse repetition rate, we only depict the RF spectrum of the laser with 10% output ratio. The RF spectrum shown in Fig. 2(b) indicates a fundamental pulse repetition rate of 586 MHz with 84 dB signal-to-noise ratio (SNR). The result is directly measured by the SA with 100 Hz resolution bandwidth (RBW), 100 Hz video bandwidth (VBW) and 100 kHz span. Figure. 2(c) depicts the RF spectrum of harmonics in a broad frequency span of 20 GHz limited by the bandwidth of our photodetector. The gain fiber used in the experiment is Liekki Er80-4/125-PM which has a normal group-velocity dispersion (GVD) of 20.5 fs<sup>2</sup>/mm at 1552 nm. The PM980-HP fiber has an abnormal GVD of -14.8 fs<sup>2</sup>/mm. The net cavity dispersion is calculated to be -1300 fs<sup>2</sup> which indicates the laser operates in the stretched-pulse regime. The polarization state of the optical pulses is linearly polarized with a degree of polarization (DOP) of 97.97%. After the pulses passing through the PM isolator, the DOP increases to 99.87%. Due to the birefringence effect of the PM fibers, the coupling efficiency between the pulses along the two axes is quite low. Therefore while pumped by an appropriate power, the MLL can maintain its polarization state.

### 3. Phase Noise and Timing Jitter at Different Harmonic Frequencies

In this section we investigate the influence of the harmonic order  $k$  on phase noise and timing jitter. Figure 3(a) presents the measured timing jitters, from which we can see that the timing jitter rapidly reduces to 62 fs from 145.95 fs when  $k$  grows to 5, then it fluctuates around 60 fs when  $k$  is above 5. Here we substitute Eqs. (3), (5) into (6) to obtain the fitting function Eq. (7), which is used to fit the experimental data.

$$\Delta t_k = \sqrt{A/k^2 + B}, \quad (7)$$

where

$$A = \int_{-\infty}^{+\infty} |f(\omega)|^2 [\delta(\omega_k) + S_I(\omega_k)] d\omega, \quad (7a)$$

$$B = (2\pi)^2 \int_{-\infty}^{+\infty} |f(\omega)|^2 S_{\Delta T}(\omega_k) d\omega. \quad (7b)$$

We find that the experimental data is in reasonable agreement with the fitting curve (red solid line) with  $\pm 20$  fs fluctuation. Comparing with the high-order harmonics, we think the higher timing jitters at low-order harmonics are due to the intensity noise of the MLL and RIN-coupled jitters. The noise sources is analyzed by comparing the differences between the phase noises at different harmonics. The phase noises of the 1st to 10th harmonics (the 6th cannot be measured by our SA for some unexplainable reasons) are given in Fig. 3(b)–(c). It can be seen that the slope of the phase noise at offset frequencies lower than 100 kHz progressively decreases from about -15 to -20 dB/dec, the former slope results from the RIN-jitter and the latter slope is the typical slope caused by ASE noise [1]. The variation of the slope implies that the influence on timing jitter of the RIN-jitter is gradually

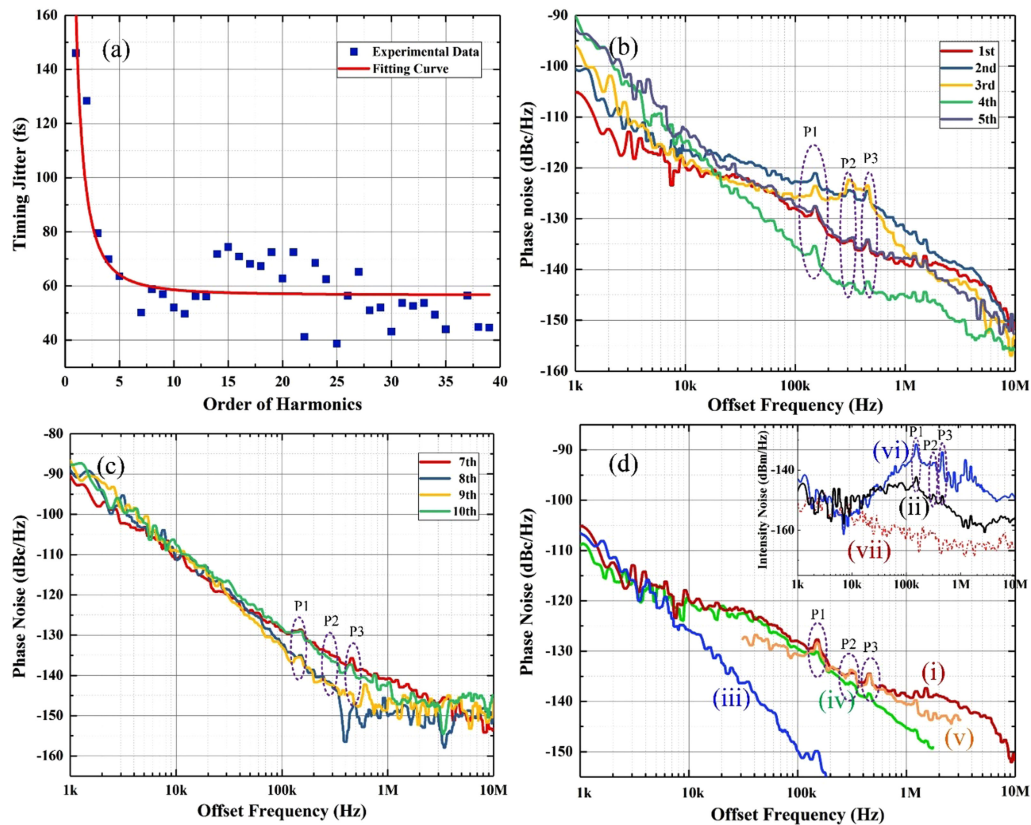


Fig. 3. (a) Variation of the timing jitter with harmonics index, (b) phase noises of 1st–5th harmonics, (c) phase noises of 7th–10th harmonics, (d) curve (i): the measured phase noise of 1st harmonic, (ii): the measured intensity noise PSD of the MLL, (iii): the noise PSD from ASE noise (direct and indirect), (iv): RIN-coupled jitter PSD from self-steepening effect and a slow saturable absorber, (v) the PSD from the direct influence of intensity noise, (vi): the intensity noise PSD of the pump light, (vii) the noise floor of the measurement system.

weakened by ASE noise. Besides, the symbolic peaks appeared in Fig. 3(b)–(d) (marked as: P1, P2, P3) proves that the phase noise is dramatically influenced by the intensity noise for low-order harmonics, which originates from the pump noise. However, for high-order harmonics these peaks disappear, which means that the effect of the intensity noise is also covered by ASE noise.

To study the origins of the timing jitter, we present the noise PSDs of different effects in Fig. 3(d). Curve (i) is the phase noise of the 1st harmonic appeared in Fig. 3(b). The intensity noise PSD of the MLL is displayed as curve (ii) in the inset (black line), curve (vi) is the intensity noise PSD of the pump light (4% of the total 327 mW pump light is coupled into the detector via a fiber coupler), and curve (vii) is the noise floor of the measuring system. We calculate curves (iii)–(v) based on Eq. (4) by using the measured PSDs of the phase noises and intensity noise of the MLL. Curves (iii) originates from ASE noise (including both the direct and indirect contributions). We divide the phase noises of the 20th, 26th, and 37th harmonics by the corresponding  $k^2$  factors and average the results to obtain curve (iii). The calculation is based on two conditions: (a) the jitter PSDs corresponding to the direct and indirect influences of ASE noise follow the same distribution at different harmonics (b) the phase noises used to calculate curve (iii) is dominant by ASE noise. The disadvantage of this method is that we cannot exactly distinguish the direct and indirect influences of the ASE noise. So is the same method used in obtaining curve (iv) from curve (ii), which corresponds to RIN-coupled jitters from both the self-steepening effect and a slow saturable absorber. Curve (v) is also calculated from curve (ii), which shows the direct influence of the intensity noise. As can be seen that in the 1–10 kHz range, both the ASE noise and RIN-coupled jitter contribute

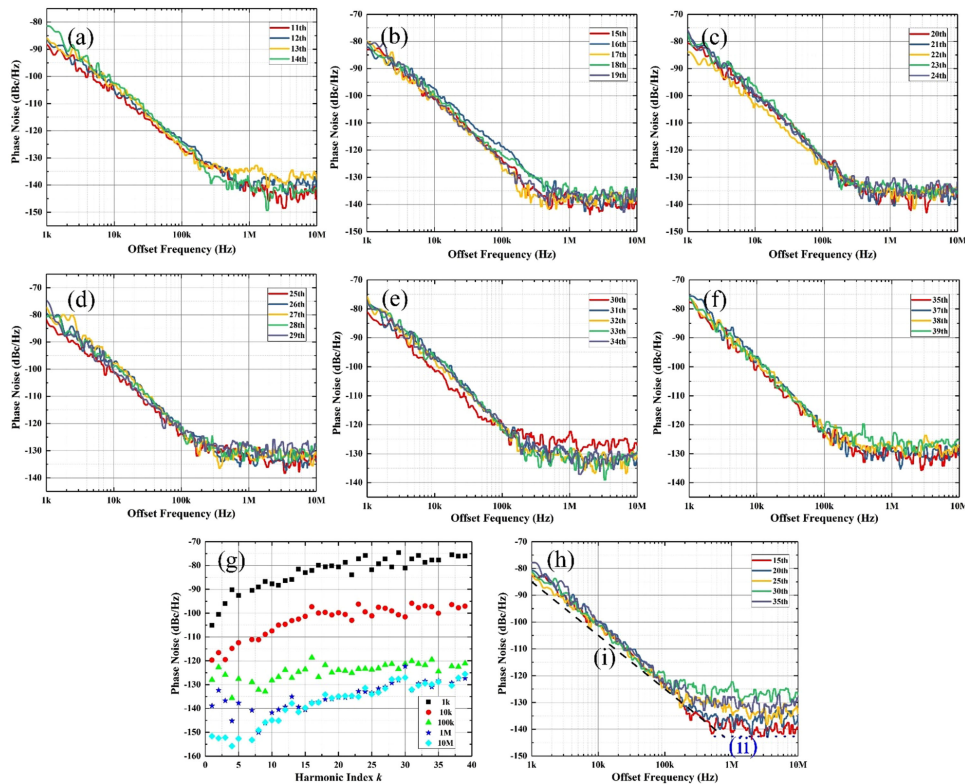


Fig. 4. (a)–(f) The phase noise curves of high-order harmonics, (g) phase noise values at certain offset frequencies for all harmonics, (h) phase noise curves of the 15th, 20th, 25th, 30th and 35th harmonics.

to the phase noise. At offset frequencies from 10 kHz to 100 kHz the RIN-jitter becomes the dominant contributor. For frequencies between 150 kHz and 800 kHz the well matching between curve (v) and curve (i) shows the intensity noise of the MLL mainly contributes to the timing jitter.

The phase noise PSDs of the 11th to 39th harmonics are shown in Fig. 4(a) to (f). It can be seen that the phase noise curves decrease following the  $1/f^2$  ( $-20$  dB/dec) slope at low offset frequencies and then enters to the flat floor region from 500 kHz. To detailedly show this behavior, we give the phase noise values at five certain offset frequencies for all harmonics in Fig. 4(g) (curve (i) for 1 kHz, (ii) for 10 kHz, (iii) for 100 kHz, (iv) for 1 MHz, and (v) for 10 MHz offset frequencies, respectively). For  $k > 10$  the deviations from (ii) to (i) and (iii) are both about 20 dB, corresponding to the  $-20$  dB/dec slope. Between (iii) and (iv), it progressively gets smaller with the increase of  $k$ . The overlapping between curves (iv) and (v) implies that the measurement is limited by the shot-noise floor of the measuring system, which is shown in Fig. 4(h) clearly, where the phase noise curves corresponding to the 15th, 20th, 25th, 30th, 35th harmonics are plotted. The simulated noise PSDs originating from ASE noise and the shot-noise floor are given as curve (i) and (ii) in Fig. 4(h), respectively. Here, we can see that for a sufficient high  $k$ , the RIN-coupled jitter is completely covered by the phase noise caused by ASE noise. Besides, the obvious increase of the phase noise at high offset frequencies shows that the shot-noise floor of the measuring system is dramatically rising while measuring higher carrier frequencies. The measurements of timing jitter and phase noise are greatly limited by the adopted measuring method, so a better measuring method, such as the balanced optical cross-correlation (BOC) [24], [25] technique, would be helpful for analyzing the origins of the timing jitter.

Based on the above analyses, we conclude that the intensity noise and the RIN-coupled jitter mainly contribute to the timing jitter for low-order harmonics. However, the phase noise cause by

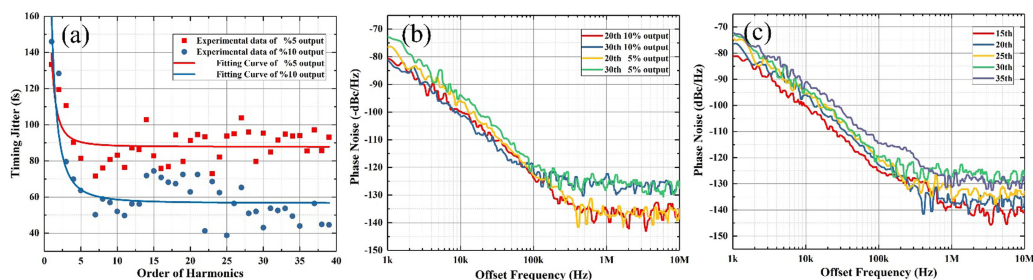


Fig. 5. (a) Comparison of timing jitters at different harmonics for laser output ratios of 5% and 10%, (b) comparison of phase noises from different MLLs at the same harmonic frequency, (c) phase noise curves corresponding to the 15th, 20th, 25th, 30th, 35th harmonics of the MLL with 5% output ratio.

ASE noise increases with  $k^2$  while the intensity noise is independent of  $k$ , the ASE noise becomes the dominant noise contribution for high-order harmonics.

#### 4. The Influence of the Output Ratio on Timing Jitter

In this section, we investigate the influence of the output ratio of the MLL on timing jitter and phase noise. The 10% OC of the original MLL is replaced by a 5% one, and the other parts of the MLL are unchanged. The measured timing jitter and the fitting curve is shown in Fig. 5(a). Obviously, the timing jitters measured with an output ratio of 5% are dramatically higher than the situation in which a 10% OC is used. In Fig. 5(b) we can see that at low offset frequencies, the phase noises of the 20th and 30th harmonics with 5% output ratio are both higher than those with 10% output ratio. For the same harmonic order of the MLLs with different output ratios, the phase noises at offset frequencies above 500 kHz overlaps, which confirms that the flat bottoms are shot-noise floors of the measuring system for different carrier frequencies.

In last section, we conclude that the timing jitter at high-order harmonic is dominated by ASE noise, which can be confirmed again by the new MLL whose phase noise curves also follow the  $-20$  dB/dec slope as shown in Fig. 5(c). Here, we use this conclusion to explain the increasing of the timing jitter and phase noise of the new MLL. It should be noted that due to the low single pulse energy, the accurate pulse duration cannot directly be measured by our autocorrelator. An amplification system can also change the pulse duration, so we use the Fourier-transform-limited full width at half maximum (FWHM) pulse duration to qualitatively analyze the timing jitter. Setting the pump power at 327 mW as before, we present the changed parameters in Table 1. Based on Eqs. 4(a)–(b), the longer pulse duration and higher net cavity dispersion increase the influence of ASE noise, which leads to the higher timing jitter and phase noise of the MLL with the 5% output ratio.

#### 5. Comparisons Between the Microwave Signals Extracted From the MLL and a Commercial SG

In this section, to show the advantages and disadvantages of the OGRFS, we compare the noise properties of the RF signals extracted from the MLL and a state-of-the-art commercial SG (model: E8257D, Keysight Technologies). The values of timing jitters are given in Table 2. The lower timing jitters of the RF signals from the SG demonstrate that the SG has a better stability than the free-running MLL in this work. The phase noises of the OGRFSs are stronger at low offset frequencies (e.g., below 30 kHz, marked by blue solid dots). However, for frequency range above about 700 kHz, the phase noises of the OGRFSs are 15, 10 and 5 dB better than those of the RF signal from the SG at 5, 10 and 20 GHz carrier frequencies, respectively. The high phase noise of OGRFS at low offset frequencies could be improved by further optimizing the parameters of the MLL and using a feedback control of the cavity length through a high speed PZT. Based on Eqs. (4a) and 4(b),

TABLE 1  
The Changed Parameters of the MLLs

Parameters	10% output ratio	5% output ratio	Variation (%)
Losses in the cavity	19	14	-26
FHWM spectral bandwidth (nm)	10.1	8.5	-15.84
Pulse duration (fs)	351	416	18.52
Intracavity single pulse energy (pJ)	33.7	37.2	10.38
Net cavity dispersion (fs <sup>2</sup> )	-1300	-2250	73.08

TABLE 2  
Timing Jitters Correspond to the MLL and the SG

Frequency (GHz)	MLL (fs)	SG (fs)
5.28	51.996	40.546
10	68.142	28.914
20	49.375	26.308

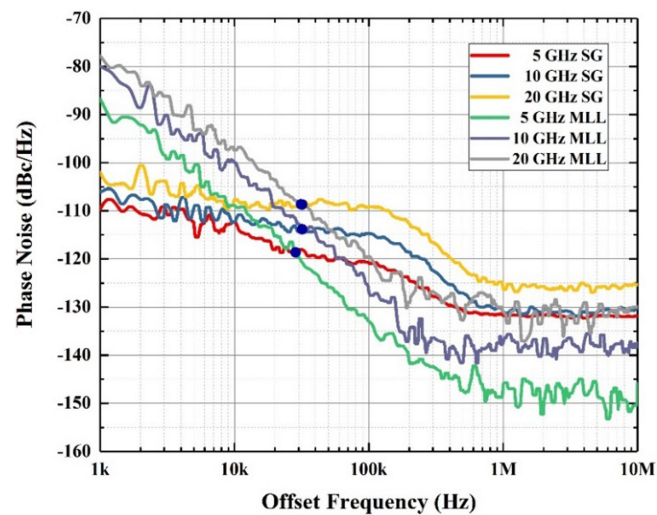


Fig. 6. Comparison of phase noises from the MLL and a commercial SG.

the optimized parameters, such as shorter pulse duration, smaller net cavity dispersion, lower losses of the cavity, and smaller spontaneous emission factor are important for reducing the phase noise from ASE noise. The optimization can be achieved by adopting different components in the laser, for example, active fibers with lower gain or SESAMs with smaller anomalous dispersion and low non-saturable loss. Besides, according to the results in Section 4, an output coupler with appropriate output ratio can also reduce the phase noise from ASE noise. Then we believe the presented passively MLL with a compact and robust structure has great potentials in generating low noise, high frequency RF signals. These OGRFSs are desired in many practical applications, such as high resolution modern radar systems.

## 6. Conclusions

In summary we design a 586 MHz free-running passively mode-locked Er-doped fiber laser and investigate its noise properties. We find that the measured timing jitter decreases with the increasing harmonic order at first and then remains constant with a  $\pm 20$  fs fluctuation. The experimental data is well consistent with the theoretical fitting curve. The noise PSDs originating from different effects are calculated and well matched with the phase noise curve of the 1st harmonic. Based on the analyses we infer that for low harmonics the higher timing jitters are dramatically affected by intensity noise of the MLL and RIN-coupled jitters, while at high harmonic frequencies the ASE noise is the dominant contributor to timing jitter. The influence of the output ratio of the MLL on timing jitter is also investigated. Although according to Eq. (4) the lower output ratio, meaning lower intracavity loss, should lead to smaller timing jitter. However, in our experiment, the timing jitter is dramatically increasing due to the variations of the other parameters caused by the lower output ratio, such as the longer pulse duration and higher net cavity dispersion. The comparison between the homemade MLL and a state-of-art commercial SG show that the OGRFS shows a better noise performance at high offset frequencies, however the higher phase noise at low offset frequencies leads to a higher timing jitter than the commercial SG. The noise properties of the OGRFSs can be improved by optimizing the parameters of the MLL, such as the pulse duration, the net cavity dispersion, and the losses of the cavity and so on. We believe that, with the further optimization, the RF signal from MLLs with high frequencies and low timing jitters would have great potential applications in modern radar systems, which has been reported in [7].

---

## References

- [1] J. Kim and Y. Song, "Ultralow-noise mode-locked fiber lasers and frequency combs: Principles, status, and applications," *Adv. Opt. Photon.*, vol. 8, no. 3, pp. 465–640, 2016.
- [2] N. R. Newbury and W. C. Swann, "Low-noise fiber-laser frequency combs (invited)," *J. Opt. Soc. Am. B*, vol. 24, no. 8, pp. 1756–1770, 2007.
- [3] J. Kim, M. J. Park, M. H. Perrott, and F. X. Kärtner, "Photonic subsampling analog-to-digital conversion of microwave signals at 40-GHz with higher than 7-ENOB resolution," *Opt. Exp.*, vol. 16, no. 21, pp. 16509–16515, 2008.
- [4] H. Leopardi *et al.*, "Single-branch Er: fiber frequency comb for precision optical metrology with 10–18 fractional instability," *Optica*, vol. 4, no. 8, pp. 879–885, 2017.
- [5] T. M. Fortier *et al.*, "Generation of ultrastable microwaves via optical frequency division," *Nat. Photon.*, vol. 5, no. 7, pp. 425–429, 2011.
- [6] V. Torres-Company and A. M. Weiner, "Optical frequency comb technology for ultra-broadband radio-frequency photonics," *Laser Photon. Rev.*, vol. 8, no. 3, pp. 368–393, 2014.
- [7] P. Ghelfi *et al.*, "A fully photonics based coherent radar system," *Nature*, vol. 507, pp. 341–345, 2014.
- [8] D. von der Linde, "Characterization of noise in continuously operating mode-locked lasers," *Appl. Phys. B*, vol. 39, no. 4, pp. 201–217, 1986.
- [9] H. A. Haus and A. Mecozzi, "Noise of mode-locked lasers," *IEEE J. Quantum Electron.*, vol. 29, no. 3, pp. 983–996, Mar. 1993.
- [10] S. Namiki and H. A. Haus, "Noise of the stretched pulse fiber laser: Part I—Theory," *IEEE J. Quantum Electron.*, vol. 33, no. 5, pp. 649–659, May 1997.
- [11] R. Paschotta, "Noise of mode-locked lasers. Part I: Numerical model," *Appl. Phys. B*, vol. 79, no. 2, pp. 153–162, 2004.
- [12] R. Paschotta, "Noise of mode-locked lasers. Part II: Timing jitter and other fluctuations," *Appl. Phys. B*, vol. 79, no. 2, pp. 163–173, 2004.
- [13] R. Paschotta, "Timing jitter and phase noise of mode-locked fiber lasers," *Opt. Exp.*, vol. 18, no. 5, pp. 5041–5054, 2010.

- [14] Y. Song, K. Jung, and J. Kim, "Impact of pulse dynamics on timing jitter in mode-locked fiber lasers," *Opt. Lett.*, vol. 36, no. 10, pp. 1761–1763, 2011.
- [15] C. Kim, S. Bae, K. Kieu, and J. Kim, "Sub-femtosecond timing jitter, all-fiber, CNT- mode-locked Er-laser at telecom wavelength," *Opt. Exp.*, vol. 21, no. 22, pp. 26533–26541, 2013.
- [16] Y. Song, C. Kim, K. Jung, H. Kim, and J. Kim, "Timing jitter optimization of mode-locked Yb-fiber lasers toward the attosecond regime," *Opt. Exp.*, vol. 19, no. 15, pp. 14518–14525, 2011.
- [17] X. Li, W. Zou, K. Wu, and J. Chen, "Timing-jitter reduction by use of a spectral filter in a broadband femtosecond fiber laser," *IEEE Photon. Technol. Lett.*, vol. 27, no. 8, pp. 911–914, Apr. 2015.
- [18] C. Ouyang *et al.*, "Observation of timing jitter reduction induced by spectral filtering in a fiber laser mode locked with a carbon nanotube-based saturable absorber," *Opt. Lett.*, vol. 35, no. 14, pp. 2320–2322, 2010.
- [19] P. Qin *et al.*, "Reduction of timing jitter and intensity noise in normal-dispersion passively mode-locked fiber lasers by narrow band-pass filtering," *Opt. Exp.*, vol. 22, no. 23, pp. 28276–28283, 2014.
- [20] Q. Qin, S. Wang, M. Hu, and Y. Song, "Effective removal of Gordon–Haus jitter in mode-locked fiber lasers," *IEEE Photon. J.*, vol. 10, no. 1, pp. 1500208–1500215, Feb. 2018.
- [21] D. Kim *et al.*, "Intensity noise suppression in mode-locked fiber lasers by double optical bandpass filtering," *Opt. Lett.*, vol. 42, no. 20, pp. 4095–4098, 2017.
- [22] K. Wu *et al.*, "Timing-jitter reduction of passively mode-locked fiber laser with a carbon nanotube saturable absorber by optimization of cavity loss," *Opt. Lett.*, vol. 35, no. 7, pp. 1085–1087, 2010.
- [23] G. Serafino *et al.*, "Phase and amplitude stability of EHF-band radar carriers generated from and active mode-locked laser," *J. Lightw. Technol.*, vol. 29, no. 23, pp. 3551–3559, Dec. 2011.
- [24] T. R. Schibli *et al.*, "Attosecond active synchronization of passively mode-locked lasers by balanced cross correlation," *Opt. Exp.*, vol. 28, no. 11, pp. 947–949, 2003.
- [25] J. Kim *et al.*, "Long-term femtosecond timing link stabilization using a single-crystal balanced cross correlator," *Opt. Lett.*, vol. 32, no. 9, pp. 1044–1046, 2007.